MDPI

Article

Design and Synthesis of Multipotent Antioxidants for Functionalization of Iron Oxide Nanoparticles

Syed Tawab Shah [1], Zaira Zaman Chowdhury [1,*], Mohd Rafie Johan [1], Irfan Anjum Badruddin [2,3], Hussein Alrobei [4] and Sarfaraz Kamangar [3]

[1] Nanotechnology and Catalysis Research Center, University of Malaya, Kuala Lumpur 50603, Malaysia; tawab_shah2003@yahoo.com (S.T.S.); mrafiej@um.edu.my (M.R.J.)

[2] Research Center for Advanced Materials Science (RCAMS), King Khalid University, P.O. Box 9004, Abha 61413, Saudi Arabia; irfan@kku.edu.sa

[3] Department of Mechanical Engineering, College of Engineering, King Khalid University, Abha 61421, Saudi Arabia; sarfaraz.kamangar@gmail.com

[4] Department of Mechanical Engineering, College of Engineering, Prince Sattam Bin Abdullaziz University, Al-Kharj 11942, Saudi Arabia; h.alrobei@psau.edu.sa

* Correspondence: dr.zaira.chowdhury@um.edu.my or zaira.chowdhury76@gmail.com; Tel.: +60-3-7967-2929 or +60-1-0267-5621

Abstract: Multipotent antioxidants (MPAO) were synthesized and characterized by FTIR, NMR. The functionalized nanoparticles (IONP@AO) were characterized by FTIR, XRD, Raman, HRTEM, FESEM, VSM, and EDX. IONP@AO1 and IONP@AO2 have average particles size of 10 nm and 11 nm, respectively. The functionalized IONP@AO has a superparamagnetic nature, with saturation magnetization of 45 emu·g^{-1}. Structure-based virtual screening of the designed MPAO was performed by PASS analysis and ADMET studies to discover and predict the molecule's potential bioactivities and safety profile before the synthesis procedure. The half-maximal inhibitory concentration (IC$_{50}$) of DPPH analysis results showed a four-fold decrease in radical scavenging by IONP@AO compared to IONP. In addition to antioxidant activity, IONP@AO showed suitable antimicrobial activities when tested on various bacterial and fungal strains. The advantage of the developed nanoantioxidants is that they have a strong affinity towards biomolecules such as enzymes, proteins, amino acids, and DNA. Thus, synthesized nanoantioxidants can be used to develop biomedicines that can act as antioxidant, antimicrobial, and anticancer agents.

Keywords: multipotent antioxidants; nanoantioxidants; functionalization; magnetite nanoparticles

1. Introduction

An antioxidant substance is a molecule or nanomaterial that can block or slow down the process of oxidation [1]. Antioxidants have also been reported to be effective as prophylatic and healing mediators for various diseases and/or toxic effects. Nanoparticles may act as nanocarriers, and have a wide range of applications, such as drug delivery. Combining material science with nanotechnology and engineering leads to significant developments that decrease the production of free radicals [2]. As a nanomaterial, nanoantioxidants can slow down the pace of auto-oxidation by trapping the chain-carrying radicals or limiting the number of events that initiate the process. Recently, several of these nanoantioxidants have shown promising results in nanomedical research [3,4].

Organic species such as proteins and lipids undergo oxidative degradation due to free radicals' chain mechanism. Alkyl radicles are converted to Peroxyl free radicals (RCOO') in the presence of oxygen. RCOO' further propagates the oxidative chain, and this phenomenon is referred to as auto-oxidation. This happens under mild conditions due to the formation of hydroperoxides as a result of peroxidation [1]. Moreover, hydroxyl and alkoxy free radicals are formed by homolytic cleavage of unstable hydroperoxides. These

free radicals are exceedingly unstable, and cause DNA damage by hitting the bases of DNA strands [5]. Reactive carbonyl species (such as 4-hydroxynonenal) are also formed by the cleavage of alkyl hydroperoxide, enhancing the oxidation process [6]. Oxidative stress is defined as an imbalance in the cell's ability to respond to Reactive Oxygen Species (ROS) by eliciting an effective antioxidant response. Biomolecules such as proteins, enzymes, and DNA are irreversibly damaged by oxidative stress, which causes genetic mutations and cell death [7].

Natural antioxidants in our diet have a significant role in lowering ROS and minimizing the risk of diseases linked to oxidative stress. Alpha-tocopherol, selenium and β-carotene supplements have been demonstrated to provide no cancer protection, or to even raise mortality risk, in clinical trials [7]. The reason behind such unexpected results is the lack of bioavailability of antioxidants to the target sites. In connection with this, nanoantioxidants present a golden opportunity, because they can be tailored to have improved properties, such as enhanced stability, compared to small molecules, with reduced chances of rapid metabolic activity, and delivery to the target sites [7]. Several nanoantixodants, such as gold nanoparticles [8], Trolox, and salvianic acid-functionalized gold nanoparticles [9–11], functionalized silver nanoparticles (AgNPs) [12], have shown enhanced DPPH radical scavenging.

Biomedical applications of magnetite nanoparticles (Fe_3O_4) have been studied extensively because of their magnetic nature, biodegradability, biocompatibility, and ease of functionalization [13]. The antioxidant properties of Fe_2O_3 nanoparticles have already been studied, showing that radical scavenging occurs due to electron transfer [14–16]. In another study, gallic acid and quercetin-functionalized magnetite nanoparticles showed synergistic organic–inorganic hybrid antioxidant properties and potent antimicrobial activity on various fungal and bacterial strains [16–18].

Numerous studies have shown that butylated hydroxytoluene (BHT) is one of the most commonly used synthetic antioxidants in the food, oil, and cosmetics industries [19]. An additional use for this synthetic antioxidant is in the field of medicine. However, certain characteristics like volatility, high-temperature instability, and toxicity, as well as safety concerns, have severely hampered the effective therapeutic application [20]. To this end, current research is focused on designing and synthesizing new BHT-derivatives to enhance antioxidant and therapeutic activities and reduce toxic side effects [21]. This study aims to design and synthesize Ethylene Glycole esters (EG-esters) of BHT-bearing antioxidant groups as an effective strategy to enhance the safety profile and solubility of BHT, and the synthesis of a new multipotent antioxidant (MPAO)-functionalized magnetic nanoantioxidant. Computational analyses were carried out prior to synthesizing MPAO to ensure that the molecules were built in accordance with the structure–activity relationship (SAR) strategy. The rule of five, polar surface area, and Lipinski parameters were used to predict absorption, distribution, metabolism, excretion, and toxicity (ADMET) properties [22]. PASS analysis was performed for MPAO to predict the potential biological activities of the molecules. MPAO were synthesized for the functionalization of the magnetite nanoparticles. The post-functionalization technique was used to synthesize magnetic nanoantioxidants. Antioxidant assay and antimicrobial activities were carried out for IONP@AO.

2. Materials and Methods

IONPs were prepared using ferric chloride hexahydrate ($FeCl_3 \cdot 6H_2O$, Sigma $\geq$ 97%), ferrous chloride tetrahydrate ($FeCl_2 \cdot 4H_2O$, Merck, (Saint Louis, MO, USA)), and ammonium hydroxide ((R and M, (28%, Shanghai, China). All chemicals were of analytical grade and were used with no extra purification. Bacterial and fungal strains were provided by Institute of Biological Sciences, Faculty of Science, University Malaya, Kuala Lumpur. The morphology of the functionalized nanoparticles was analyzed using a High-Resolution Transmission Electronic Microscope (HRTEM) (Model: JEM-2100F, JEOL, Tokyo, Japan). The system was equipped with a 200 kV field emission gun. A drop of the sample was evaporated on a C-coated Cu grid to prepare it for HRTEM analysis. The particle size was

determined using Gatan Digital Micrograph software. Cu-Kα radiation (λ = 1.54060 Å) was used for X-ray diffraction (XRD) Analysis. The range of 2θ was scanned from 10.00 to 90.00 using PANalytical X-ray diffractometer (Model: EMPYREAN, Almelo, The Netherlands). Surface functional groups were identified using Fourier-transform infrared spectroscopic analysis (Perkin Elmer, Tokyo, Japan). Energy Dispersive X-ray Analysis (EDX) (INCA Energy 200 (Oxford Inst., Hillsboro, OR, USA)) was performed under vacuum conditions with a working distance of 6 mm. Surface area method was used to calculate % composition. Raman spectra of nanoparticles were taken on Renishaw with a 514 nm Argon gas laser. Magnetic properties were measured in solid state at room temperature using vibrating-sample magnetometer (VSM) analysis (Lake Shore magnetometer, (Gloucestershire, UK)).

2.1. Computational Studies

PASS web server was used to investigate potential biological activities of MPAO. PASS is a useful tool for exploring possible bioactivities of organic molecules based on their chemical formula [23]. It employs two-dimensional molecular fragments known as multilevel neighbors of atoms (MNA) descriptors to imply that a chemical compound's biological activity is a function of its molecular structure. It calculates the prediction score for biological attributes based on the ratio of the probability of being active (Pa) to the probability of being inactive (Pi). A higher Pa value indicates that the biological feature is more likely to occur in a compound. The bioactivity of selected compounds was assessed using the Molinspiration Cheminformatics server (http://www.molinspiration.com, accessed on 15 July 2021). In addition, fragment-based virtual screening, bioactivity prediction, and data visualization are all supported by this program. Lipinski's rule of five was applied to predict ADMET and physicochemical properties.

2.2. Synthesis of MPAO1 (2-(2-(2-Hydroxyethoxy)ethoxy)ethyl 2-((3,5-Di-tert-butyl-4-hydroxybenzyl)thio)acetate)

Triethylene glycol was added to a solution of 2-((3,5-di-tert-butyl-4-hydroxybenzyl)thio) acetic acid (2 g) in dry toluene (5 mL), p-Toluenesulfonic acid (PTSA) (0.02 g) was used as a catalyst. The reaction mixture was refluxed for 8 h, as shown in Figure 1A. Dean Stark apparatus was used to remove water produced during the reaction. The catalyst and unreacted materials were removed by filtration and then washed with distilled water. The mixture was dried by using anhydrous sodium sulphate. The precipitates obtained were filtered and dried at room temperature (RT) and recrystallized from the appropriate solvent.
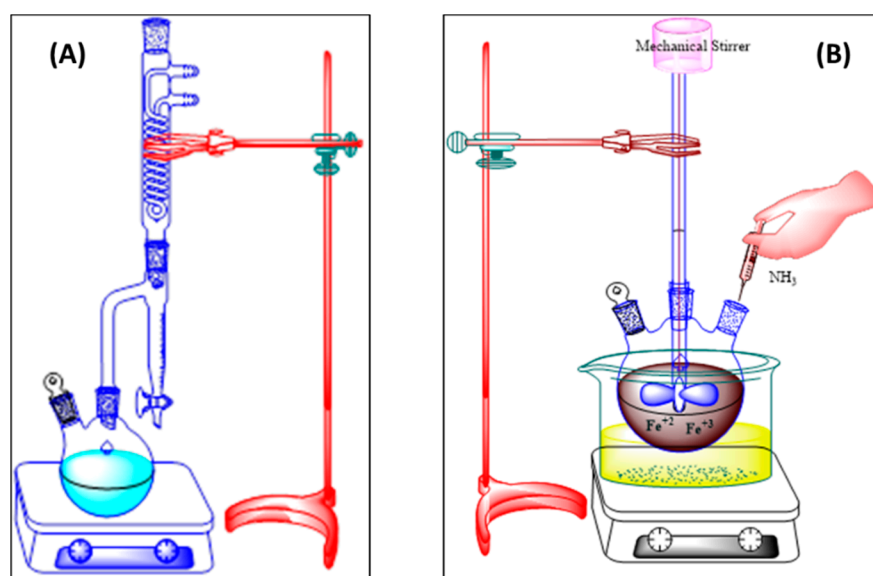

Figure 1. (**A**) Synthesis of multipotent antioxidants; (**B**) synthesis of IONP.

Chemical Formula: $C_{23}H_{38}O_6S$, Molecular Weight: 442.61, ^{1}H NMR (ppm) (600 MHz, CDCl$_3$) δ 7.04 (s, 2H), 5.10 (s, 1H), 4.23 (s, 2H), 3.71 (s, 2H), 3.65 (s, 4H), 3.60 (s, 4H), 3.52 (s, 2H), 3.08 (s, 2H), 1.71 (s, 1H), 1.36 (s, 18H). ^{13}C NMR (ppm) (151 MHz, CDCl$_3$) δ 170.58, 152.74, 125.86, 72.51, 70.62, 70.36, 69.02, 64.14, 61.78, 36.82, 34.31, 32.57, 30.29.

2.3. Synthesis of MPAO2 (2-(2-(2-(2-Hydroxyethoxy)ethoxy)ethoxy)ethyl 2-((3,5-Di-tert-butyl-4-hydroxybenzyl)thio)acetate)

Tetraethylene glycol was added to a solution of 2-((3,5-di-tert-butyl-4-hydroxybenzyl) thio)acetic acid (2 g) in dry toluene (5 mL), PTSA (0.02 g) was used as a catalyst. The reaction mixture was refluxed for 8 h. Dean Stark apparatus was used to remove water produced during the reaction as shown in Scheme 1. The catalyst and unreacted materials were removed by filtration and then washed with distilled water. The mixture was dried by using anhyderous sodium sulphate. The precipitates obtained were filtered and dried at RT and recrystallized from the appropriate solvent.
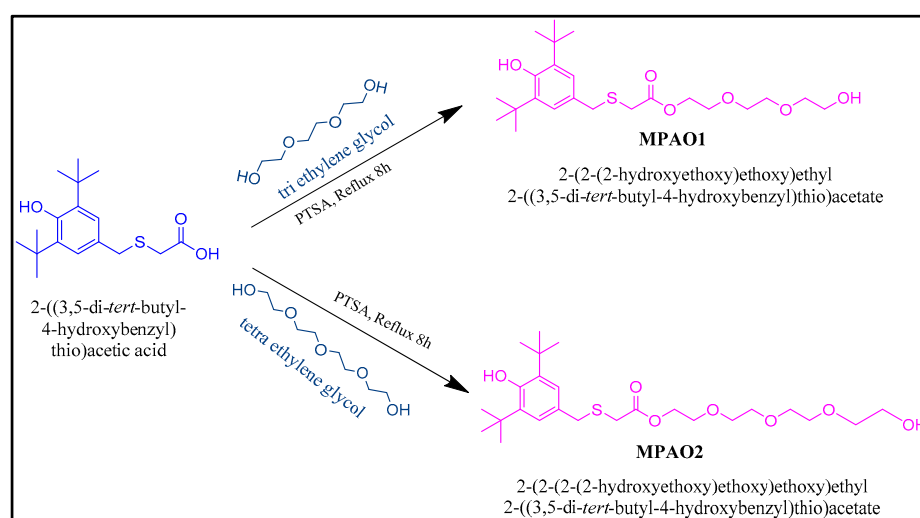
Scheme 1. Synthesis of MPAO.

Chemical Formula: $C_{25}H_{42}O_7S$, Molecular Weight: 486.66, ^{1}H NMR (ppm) (396 MHz, CDCl$_3$-D) δ = 7.16 (d), 7.10–7.06 (m), 5.08 (d), 4.08 (q), 3.75 (s), 2.01 (s), 2.01 (s), 1.39 (s), 1.39 (s), 1.22 (t), 1.22 (t). ^{13}C NMR (100 MHz, CDCl$_3$) (ppm) δ = 173.68, 171.27, 153.13, 136.08, 127.35, 125.95, 77.44, 77.33, 77.12, 76.80, 60.47, 36.86, 34.35, 32.44, 30.28, 21.09, 14.23, 1.06. Synthesis procedure is summarized Scheme 1. All Characterizations are included in Supplementary Materials (See Figure S1–S5).

2.4. Preparation of Magnetite Nanoparticles (IONP)

IONP was synthesized by combining ferrous and ferric chlorides at a 1:1.5 ratio. In 100 mL of deionized water, the salt mixture was dissolved, and ammonium hydroxide solution (3M) was added at a 5 mL/min rate until the pH reached 11. The mixture was continuously stirred at 600 rpm by using a mechanical stirrer, as shown in Figure 1B. The reaction mixture was kept at 80 °C for 90 min with continuous stirring. The product obtained was separated by using magnetic decantation, rinsed thoroughly with deionized water and ethanol. The black precipitates obtained were freeze dried to obtain a black powder of magnetite nanoparticles.

2.5. Post-Functionalization

Synthesis of IONP@AOx

The synthesized MPAO1 was dissolved in ethanol and was mixed with the ethanolic suspension of IONPs. To obtain IONP@AO1, the reaction mixture was sonicated for 20 min and then stirred for 24 h. Deionized water and ethanol (C_2H_5OH) was used to

rinse the precipitates prior to freeze-drying thoroughly. To synthesize IONP@AO2, the same process was repeated with MPAO2. Figure 2 shows a schematic illustration of IONP functionalization.
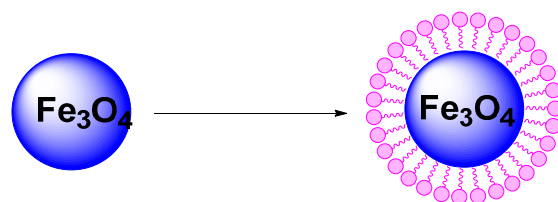

Figure 2. Functionalization of IONP with multipotent antioxidants.

2.6. DPPH Assay

Various chemical-based techniques can be used to assess antioxidant activity. Either electron transfer or H atom transfer is used in these tests, depending on the outcome of the reaction. The ability of IONP@AO to scavenge free radicals was assessed using the DPPH test, which relies on electron transfer [24]. The antioxidant properties of nanoparticles were investigated using a modified DPPH assay [24,25]. Methanolic suspension of the sample (300 µL) and 1 mL of methanolic solution of DPPH (0.2 mM) were mixed in 1 cm quartz cuvettes. The readings were taken after thirty minutes. The absorbance was continuously observed at 517 nm. Each experiment was repeated twice. Every reading was noted after exactly 30 min of mixing with DPPH solution. The free radical scavenging capacity of the samples was calculated by using Equation (1):

$$\text{percent Inhibition } (\%) = \frac{(Ac - As)}{Ac} \times 100 \tag{1}$$

where As = absorbance of sample/positive control and Ac = Absorbance of DPPH solution (Control). IC_{50} was calculated by plotting percent inhibition vs. various concentrations.

2.7. Antimicrobial Activity

2.7.1. Determination of Antibacterial Activity

Antibacterial assay was performed by agar well diffusion method [26]. Precultures of *Staphylococcus aureus* (ATCC 12600), *Bacillus subtilis* (ATCC 6051), and *Escherichia coli* (ATCC 11775) were spread on the surface of nutrient agar (NA) agar, and wells (diameter = 6 mm) were filled with 100 µL of the test samples (100 mg/mL) and incubated at 37 °C for 24 h. Sterile distilled water was used as negative control while ampicillin (100 mg/mL) and streptomycin (100 mg/disc) were positive controls for Gram-negative and Gram-positive bacterial strains, respectively. The antibacterial properties were evaluated by measuring halo (inhibition) zones.

2.7.2. Determination of Antifungal Activity

Antifungal assay for functionalized and unfunctionalized IONPs was performed using *Aspergillus niger* (ATCC 16888), a filamentous fungus (multicellular); *Saccharomyces cerevisiae* (ATCC 18824), a yeast (unicellular); *Candida albican* (ATCC 18804), a yeast; and *Trichoderma* spp. (ATCC 12668) by using the well diffusion method. Plates of potato dextrose agar were inoculated with fungal strains. The wells were dug on the potato dextrose agar (PDA) plate and filled it with 100 microliters of samples (100 mg/mL). The experiment was conducted in aseptic environment. The plates were incubated at 25 °C for 48 h. Sterile distilled water and Nystatin (100 mg/mL) were used as a negative and positive controls, respectively. The inhibition percentage of growth of mycelia (*POI*) was calculated using Equation (2):

$$POI = \frac{R1 - R2}{R1} \times 100 \tag{2}$$

where

*R*1 = Colony radius of the pathogens opposed to antagonist agent.
*R*2 = Colony radius of the pathogen towards the antagonist agent.

3. Results

3.1. FTIR Analysis

The FTIR spectra of IONP and IONP@AO are shown in Figure 3. Magnetite was observed in the nanoparticle samples, with a strong absorption at 551, 555, and 562 cm^{-1} for IONP, IONP@AO1, and IONP@AO2, respectively. The peak observed at 3100–3200 cm^{-1} is due to stretching vibration of −OH. The peak at 1621 cm^{-1} confirms the presence of carbonyl groups in both samples of IONP@AO [27].
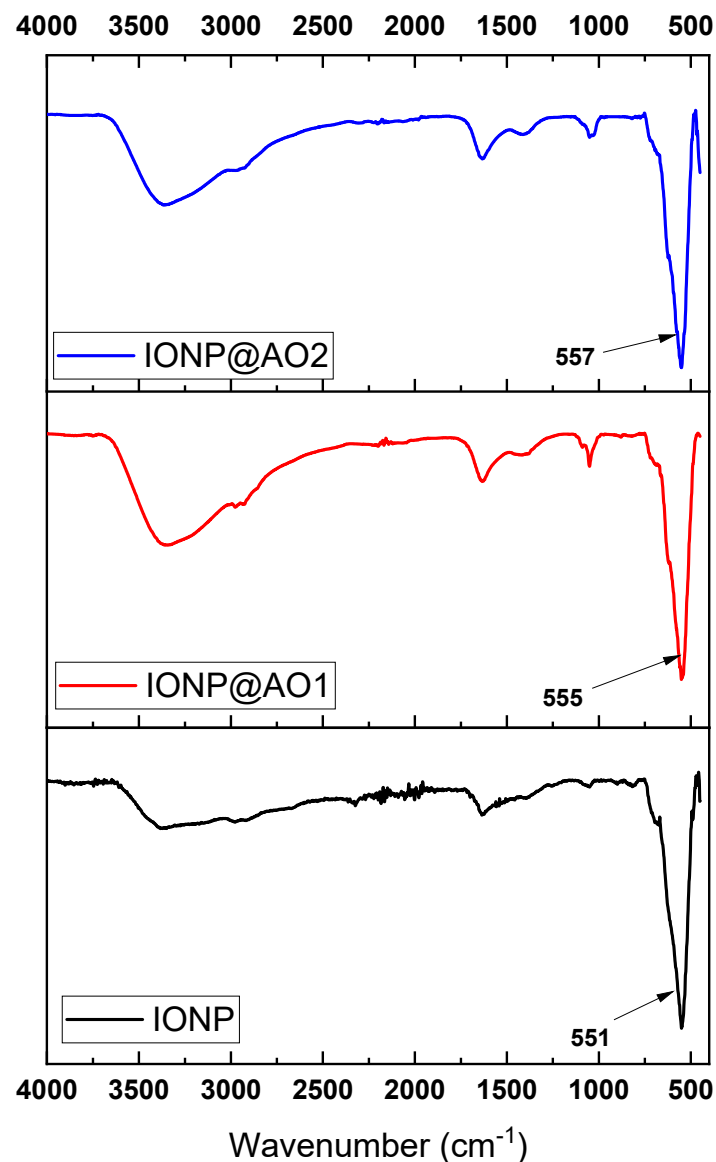

Figure 3. FTIR spectra of unfunctionalized IONP and functionalized IONP@AO.

3.2. Raman Analysis

Spectra obtained from Raman analysis are presented in Figure 4. The main band at 671 cm^{-1} (A1g) verifies the presence of magnetite [28]. IONP@AO has a main band centered at 675 cm^{-1}, and the peaks at ca. 478 cm^{-1} and 343 cm^{-1} are due to the A1g, T2g, and Eg vibration bands of magnetite. Moreover, no peaks were observed for maghemite in the Raman spectra of either functionalized or unfunctionalized IONP [29,30].
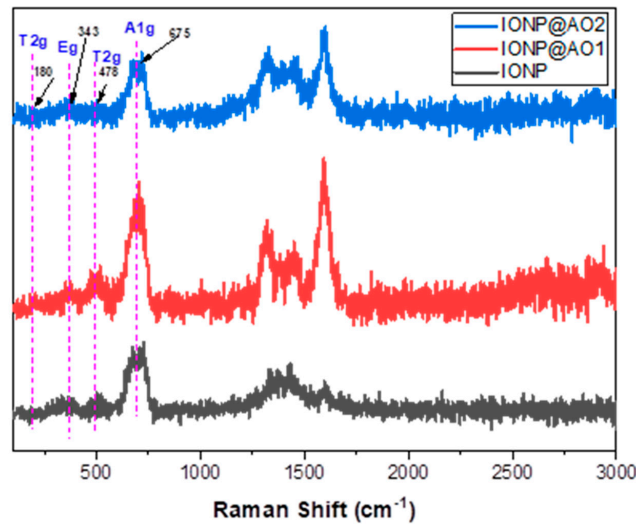
Figure 4. Raman spectroscopy analysis of unfunctionalized IONP and functionalized IONP@AO.

3.3. XRD Analysis

Figure 5 shows the XRD spectra of the samples. All the samples demonstrated the diffraction peaks at the 2θ value of 30, 25, 43, 57 and 63, which correspond to [220], [311], [400], [422] and [440] Brag reflections, respectively. The XRD pattern verified the magnetite nanoparticles with cubic inverse spinel structure (JCPDS No 96-101-1033). Moreover, the diffractions at 210, 213, and 300 were not observed, which verified that maghemite is absent in all samples. It can be seen that the functionalization of IONP did not change its phase.
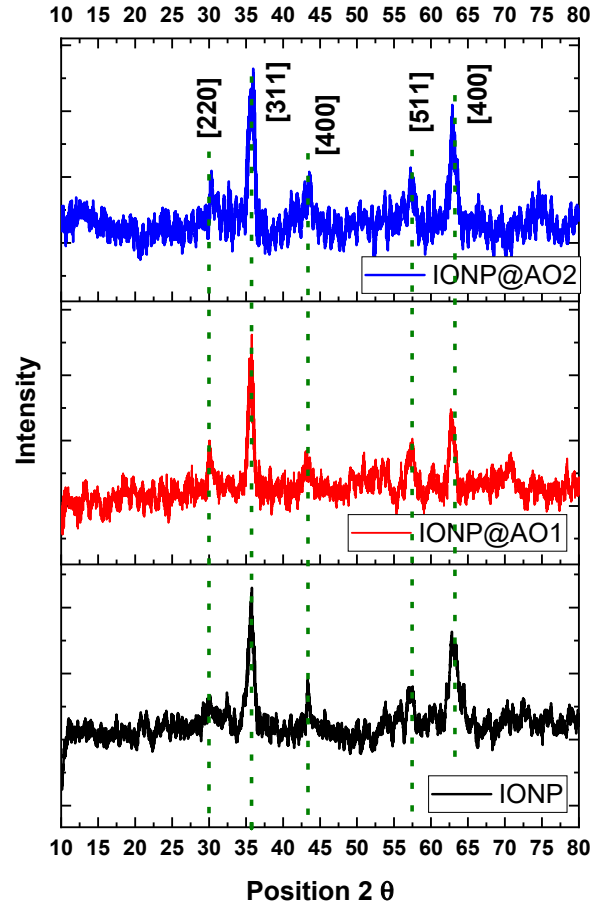

Figure 5. XRD spectra unfunctionalized IONP and functionalized IONP@AO.

3.4. Magnetic Properties

A vibrating sample magnetometer (VSM) was used to determine saturated mass magnetization. Values of 64.19 and 45 emu·g^{-1} (Table 1) were given for bare iron oxide nanoparticles and functionalized IONP@AO, respectively. Figure 6 displays the hysteresis loop as a function of the magnetic field at an ambient temperature. All samples showed superparamagnetic behavior, and their saturation magnetization was lower than magnetite in bulk (92 emu·g^{-1}) [31]. Functionalized IONP@AO1 and IONP@AO2 saturation magnetization was reduced compared to unfunctionalized IONP, probably because of the presence of organic species on its surface [32–34].

Table 1. Magnetic properties of unfunctionalized IONP and functionalized IONP@AO.

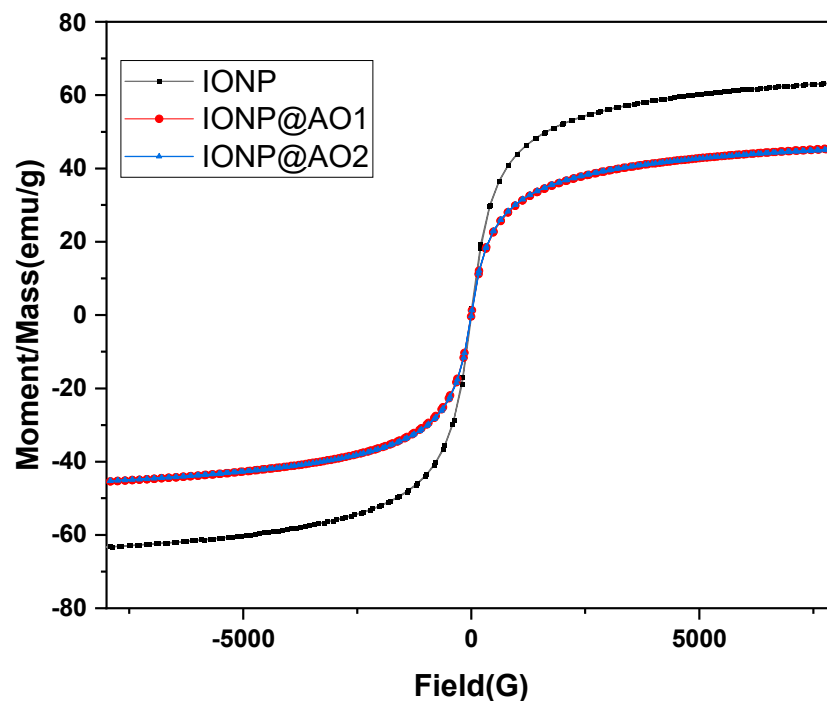| Sample	Ms
IONP	64.19
IONP@AO1	45.43
IONP@AO2	45.25

Figure 6. Room-temperature hysteresis loops for unfunctionalized IONP and functionalized IONP@AO.

3.5. Morphology and Structure

The morphology of the functionalized and unfunctionalized IONP was studied by high-resolution transmission electron microscopy (HRTEM). Figure 7 shows the high-resolution electron images and size distribution of the nanoparticles. The analysis of the TEM images revealed that particle size on average was 10.07, 10.08 nm, and 11 nm for IONP, IONP@AO1, and IONP@AO2, respectively. The results show that particles were distributed uniformly and had a spherical shape. The agglomeration of nanoparticles was because of the superparamagnetic behavior of the nanoparticles. The crystal lattice fringe spacing was 0.26 nm, which corresponds to the (220) lattice plane of IONP [35].
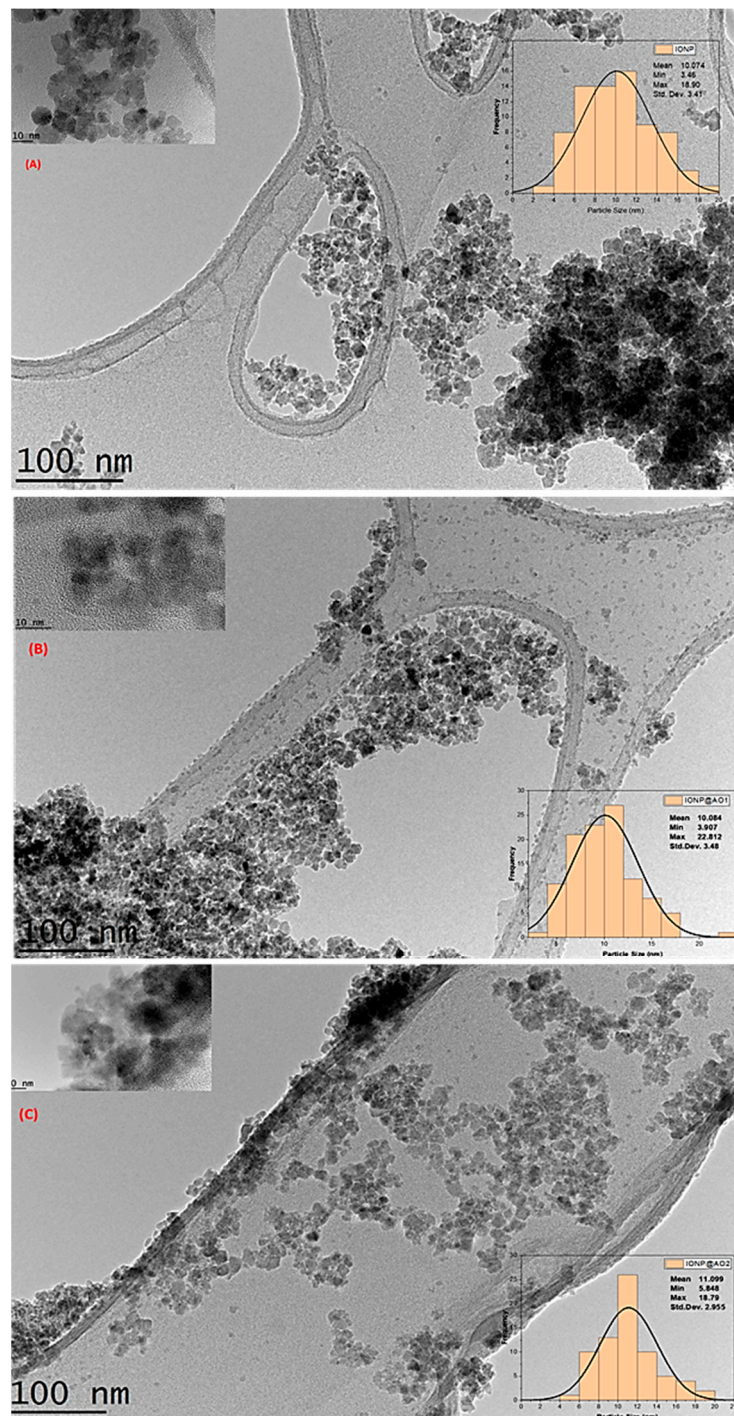
Figure 7. HRTEM images: (**A**) unfunctionalized IONP; (**B**) functionalized IONP@AO1; (**C**) functionalized IONP@AO2. Insets show particle size distribution.

3.6. EDX Analysis

Table 2 presents the elemental composition of the samples. Magnetite nanoparticles showed Fe and O signals in all samples, whereas the C and S signals were due to organic moieties present in IONP@AO1 and IONP@AO2. Furthermore, EDX mapping confirmed the uniform distribution of the elements present in the samples. The mapping of C and S was uniform, as shown in Figure 8, confirming that nanoparticles were functionalized well.

Table 2. Elemental composition analysis employing SEM–EDX energy-dispersive X-ray spectrum.

Sample	Fe	O	C	S
IONP	69.4	30.6	-	-
IONP@AO1	61.7	25.1	13.4	0.1
IONP@AO2	65.9	25.4	8.3	0.1
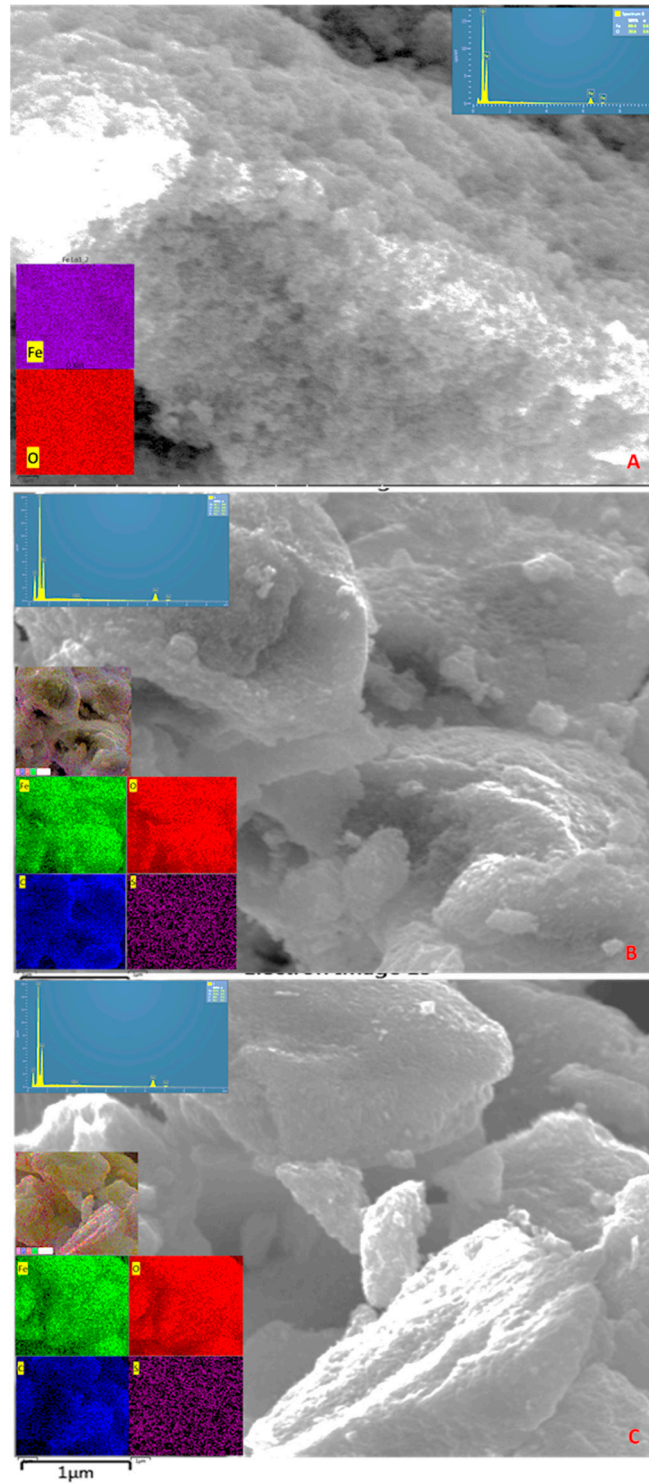
Figure 8. EDX of (**A**) IONP, (**B**) IONP@AO1, and (**C**) IONP@AO2.

3.7. Computational Analysis

3.7.1. ADMET Studies

The physicochemical characteristics of synthesized MPAO were analyzed and calculated based on Lipinski's rule of five (Mol. Weight $\leq$ 500 Da, Log P $\leq$ 5, H-bond donor $\leq$ 5 and H bond accepter $\leq$ 10). Table 3 shows the properties predicted by ADMET. Figure 10A–D show the molecular lipophilicity potential (MLP) in order to visualize hydrophobicity (blue and violet colors) and hydrophilicity (red and orange) on the molecular surface. The miLogP method was used for MLP calculation from atomic hydrophobicity contributions; this method is the same as calculating the octanol–water partition coefficient (logP). MLP is valuable for rationalizing a variety of molecular ADME properties (such as a membrane penetration or plasma–protein binding). The 3D distribution of hydrophobicity on the molecule's surface is helpful for explaining the difference in the observed ADME properties of molecules having the same logP values [36]. The 3D parameter provides more information than logP expressed by just a single value. Figure 9 presents the boiled egg predictive model of lipophilicity (WLOGP) and polarity (tPSA) computation. The white region of the plot shows a higher probability of absorption in the gastrointestinal tract, while the yellow region (yolk) suggests a higher probability of permeation in the brain [37,38].
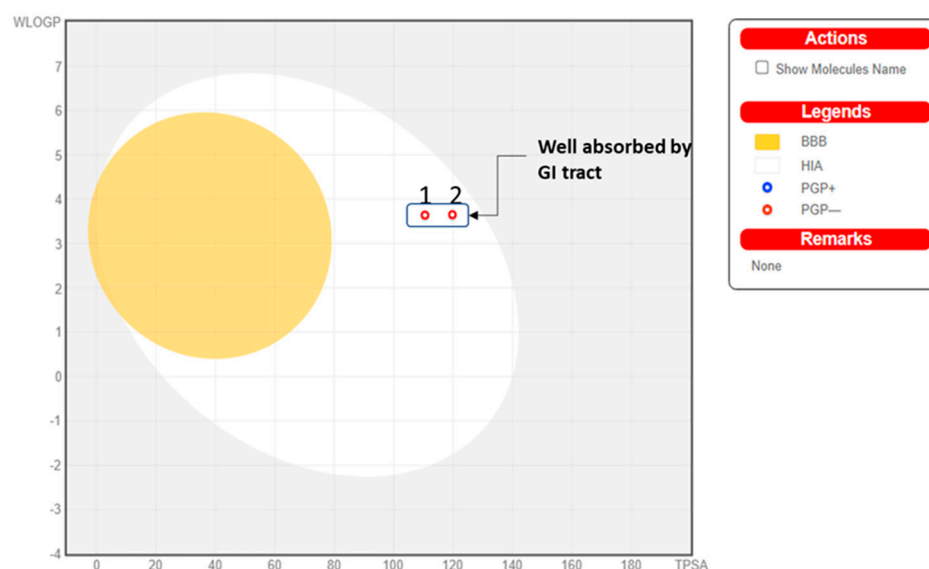

Figure 9. Boiled egg predictive model of MPAO.

Table 3. Predicted absorption, distribution, metabolism, excretion, and toxicity (ADMET) properties from computational analysis.

Physicochemical Properties		
Formula	$C_{23}H_{38}O_6S$	$C_{25}H_{42}O_7S$
MW	442.61	486.66
#Heavy atoms	30	33
#Aromatic heavy atoms	6	6
Fraction Csp3	0.7	0.72
#Rotatable bonds	15	18
#H-bond acceptors	6	7
#H-bond donors	2	2
MR	122.63	133.33
TPSA	110.52	119.75

Table 3. *Cont.*

Lipophilicity		
iLOGP	4.57	4.78
XLOGP3	4.3	4.15
WLOGP	3.64	3.65
MLOGP	2.39	2.01
Silicos-IT Log P	5.47	5.89
Consensus Log P	4.07	4.1
Water Solubility		
ESOL Log S	−4.45	−4.42
ESOL Solubility (mg/mL)	1.57×10^{-2}	1.86×10^{-2}
ESOL Solubility (mol/L)	3.54×10^{-5}	3.82×10^{-5}
ESOL Class	Moderately soluble	Moderately soluble
Ali Log S	−6.33	−6.37
Ali Solubility (mg/mL)	2.05×10^{-4}	2.06×10^{-4}
Ali Solubility (mol/L)	4.63×10^{-7}	4.24×10^{-7}
Ali Class	Poorly soluble	Poorly soluble
Silicos-IT LogSw	−6.07	−6.57
Silicos-IT Solubility (mg/mL)	3.77×10^{-4}	1.30×10^{-4}
Silicos-IT Solubility (mol/L)	8.51×10^{-7}	2.67×10^{-7}
Silicos-IT class	Poorly soluble	Poorly soluble
Pharmacokinetics		
GI absorption	High	High
BBB permeant	No	No
Pgp substrate	No	No
CYP1A2 inhibitor	No	No
CYP2C19 inhibitor	No	No
CYP2C9 inhibitor	No	No
CYP2D6 inhibitor	Yes	No
CYP3A4 inhibitor	Yes	Yes
log Kp (cm/s)	−5.95	−6.32
Druglikeness		
Lipinski #violations	0	0
Ghose #violations	0	3
Veber #violations	1	1
Egan #violations	0	0
Muegge #violations	0	1
Bioavailability Score	0.55	0.55
Medicinal Chemistry		
PAINS #alerts	0	0
Brenk #alerts	0	0
Leadlikeness #violations	3	3
Synthetic Accessibility	4.04	4.32

3.7.2. PASS Analysis

PASS predictions forecasted the bioactivities of synthesized compounds. The multilevel neighbor of atoms (MNA) descriptors (2D molecular fragment) are used in PASS studies to describe biological activity is a molecular structure-function. The predictive score for activities is given as the probability ratios between 'probability to be active (Pa)' and 'probability of being non-active (Pi)'. Higher values of Pa represent higher activity of organic molecules. Table 4 shows the selected bioactivities with higher Pa values when Pa > Pi. Figure 10A–D show the polar surface area and molecular lipophilicity potential (MLP) of MPAO.

Table 4. Part of the predicted biological activity spectra of the MPAO based on PASS prediction software.

	MPAO	
[a] **Pa**	[b] **Pi**	**Biological Activity**
0.410	0.017	Free radical scavenger
0.420	0.030	Lipid peroxidase inhibitor
0.301	0.023	Antioxidant
0.308	0.078	Antifungal
0.262	0.077	Antibacterial

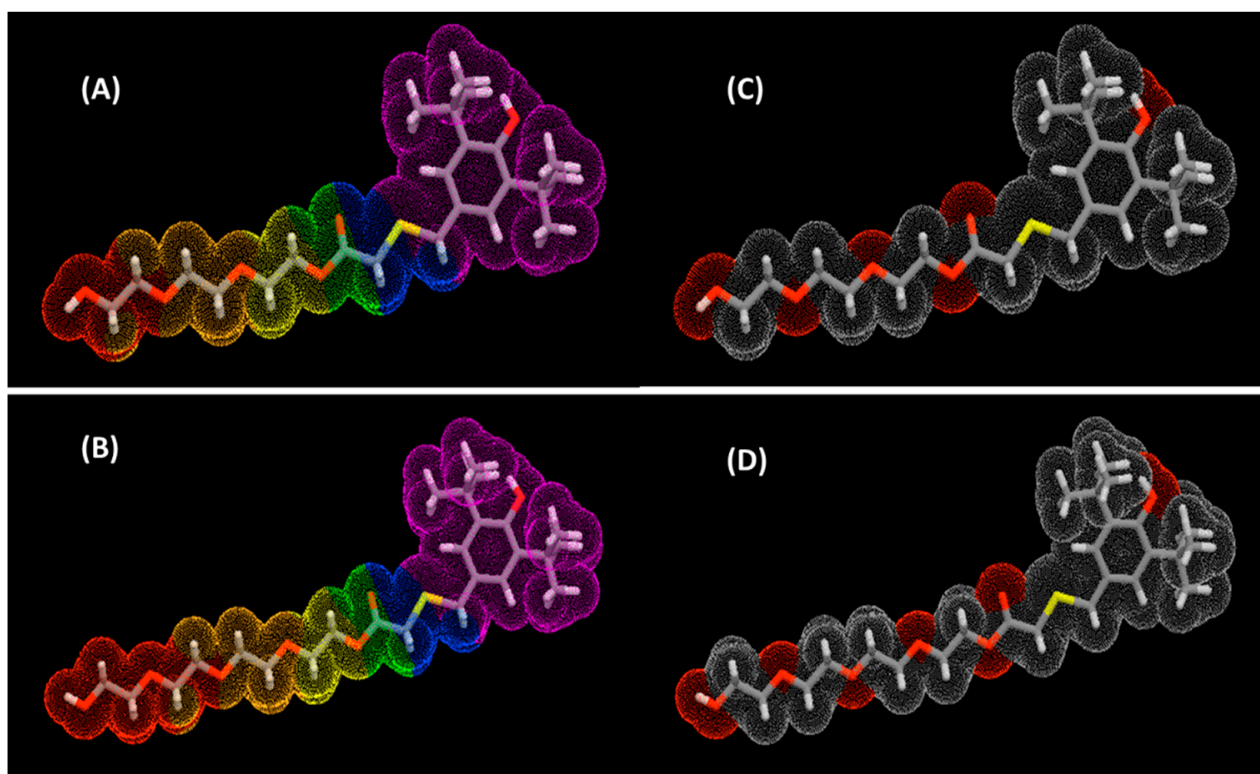[a]—Probability "to be active". [b]—Probability "to be inactive".

Figure 10. (**A**,**B**) Molecular lipophilicity potential (MLP); (**C**,**D**) polar surface area.

Antioxidant values and other predicted bioactivities of the MPAO having Pa > 0.7 suggest that nanomaterial functionalized with MPAO could display enhanced activities compared to nanoparticles without functionalization. This is owing to its biocompatibility, which can assist in the drug transportation system and bioimaging. Biological testing verified the predicted results.

3.8. Antioxidant Activity

Figure 11 shows UV-visible spectra of the samples. At 517 nm, there is a reduction in peak intensity. The reduction in pak height was used to calculate the free radical scavenging percentage. The IC50 value (Table 5) and the percentage inhibition of stable free radical DPPH for the synthesized nanoantioxidants were found to be 1.5 ± 0.002 mg/mL and 79% for IONP@AO1 and 2.4 ± 0.002 mg/mL and 58% for IONP@AO2 at a 10^{-4} M, which is two to four times greater than with bare iron oxide nanoparticles (IC50 4.7 ± 0.002 mg/mL and 50%), which was used as a refence in this experiment. In comparison to IONP, IONP@AO exhibited a greater capacity for free radical scavenging. The electron transfer reaction between IONP@AO and DPPH was most likely responsible for the increased radical scavenging. Nanoparticles and MPAO promote good radical scavenging.
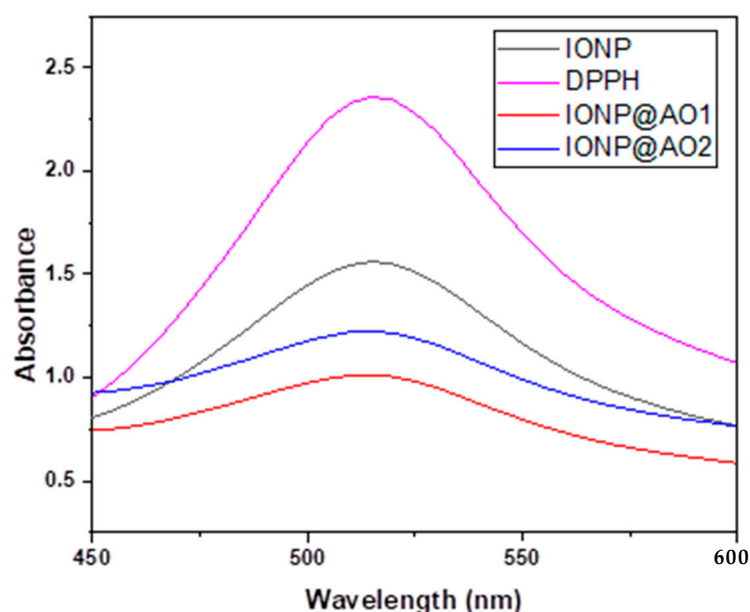

Figure 11. UV-visible spectra, DPPH Scavenging percentage by IONP@AO at different concentrations.

Table 5. IC50 of IONP@AO.

IC50 [a] Values (mg) $\pm$ S.E.M [b] and Max. Inhibition %		
Sample	**IC50 mg/mL**	**% Inhibition**
IONP	5 mg	4.7 ± 0.002	50
IONP@AO1	5 mg	1.5 ± 0.002	79
IONP@AO2	5 mg	2.4 ± 0.002	58

[a]—IC50, 50% effective concentration. [b]—S.E.M, standard error of the mean.

3.9. Antibacterial Activity

The results of the agar well diffusion technique are summarized in Figure 12A. The percentage inhibition of bacteria's diameter growth (PIGD) is plotted against the 100 mg/mL experimental sample concentration. Antibacterial activity against Gram-negative and Gram-positive species of bacteria was observed for functionalized IONP@AO. For the most effective samples, the minimal inhibitory concentration was estimated. IONP@AO exhibited distinct bactericidal effects against Gram-positive and Gram-negative bacteria. Different varieties of bacteria had distinct types of cell walls leading to this finding. Gram-positive bacteria have a relatively substantial, thicker peptidoglycan layer (10–30 nm) on their surface, while Gram-negative bacteria have an additional outer layer with a thin layer of peptidoglycan (10 nm). IONP@AO has been shown to have varying degrees of antibacterial activity against a range of bacterial species. Internalization of functionalized IONPs within the cells happens when IONP@AO is introduced to bacterial strains,

resulting in inhibition. Because the 1,4 glycosidic linkages are broken, the cell wall is eventually destroyed.
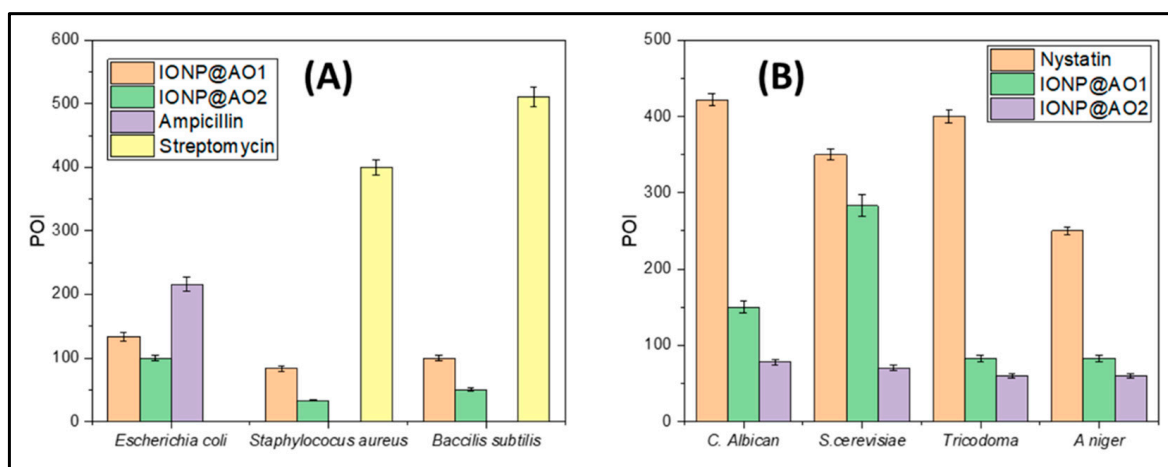

Figure 12. Percentage of inhibition (POI) of (**A**) bacterial growth and (**B**) fungal growth after treatment with IONP@AO.

3.10. Antifungal Activity

The results obtained for the agar-well diffusion method are illustrated in Figure 12B. Antifungal activity was observed for *Aspergillus Niger*, *Trichoderma* spp., *Candida albicans*, and *Saccharomyces cerevisiae*. For *Aspergillus Niger*, *Saccharomyces cerevisiae*, and *Candida albicans*, IONP@AO showed enhanced antifungal activity. It exhibited reduced antifungal activity for *Trichoderma* sp. Functionalized nanoparticles prompted cellular damage and death of the treated cells eventually. In general, ultra-small nanoparticles have fungicidal activities. Nevertheless, it is determined by the synthesis protocol and physicochemical attributes of the nanoparticles.

4. Conclusions

IONP functionalized with MPAO was successfully synthesized using post-functionalization procedures. The possible bioactivities and safety profile of MPAO molecule were studied and predicted before the synthesis procedure by PASS analysis and ADMET studies using the structure-based virtual screening technique. The average particle size was 10 nm and 11 nm for functionalized IONP@AO1 and IONP@AO2, respectively. The synthesized nanoparticles were analyzed using XRD, FTIR, VSM, EDX, HRTEM, and Raman analysis. It was observed that magnetite retained its properties after functionalization with MPAO. All samples showed superparamagnetic behavior confirmed by VSM. IONP@AO1 showed better radical scavenging and antimicrobial activities compared to IONP@AO2 and IONP. MPAO functionalized IONP showed promising free radical scavenging properties and antimicrobial properties.

Conflicts of Interest: The authors declare no conflict of interest.

References

1. Ingold, K.U.; Pratt, D.A. Advances in radical-trapping antioxidant chemistry in the 21st century: A kinetics and mechanisms perspective. *Chem. Rev.* **2014**, *114*, 9022–9046. [CrossRef] [PubMed]
2. Eftekhari, A.; Ahmadian, E.; Panahi-Azar, V.; Hosseini, H.; Tabibiazar, M.; Maleki Dizaj, S. Hepatoprotective and free radical scavenging actions of quercetin nanoparticles on aflatoxin b1-induced liver damage: In vitro/in vivo studies. *Artif. Cells Nanomed. Biotechnol.* **2018**, *46*, 411–420. [CrossRef] [PubMed]
3. Hasanzadeh, M.; Mokhtari, F.; Shadjou, N.; Eftekhari, A.; Mokhtarzadeh, A.; Jouyban-Gharamaleki, V.; Mahboob, S. Poly arginine-graphene quantum dots as a biocompatible and non-toxic nanocomposite: Layer-by-layer electrochemical preparation, characterization and non-invasive malondialdehyde sensory application in exhaled breath condensate. *Mater. Sci. Eng. C* **2017**, *75*, 247–258. [CrossRef] [PubMed]
4. Hasanzadeh, M.; Tagi, S.; Solhi, E.; Mokhtarzadeh, A.; Shadjou, N.; Eftekhari, A.; Mahboob, S. An innovative immunosensor for ultrasensitive detection of breast cancer specific carbohydrate (ca 15-3) in unprocessed human plasma and mcf-7 breast cancer cell lysates using gold nanospear electrochemically assembled onto thiolated graphene quantum dots. *Int. J. Biol. Macromol.* **2018**, *114*, 1008–1017. [CrossRef]
5. Cadet, J.; Wagner, J.R. Oxidatively generated base damage to cellular DNA by hydroxyl radical and one-electron oxidants: Similarities and differences. *Arch. Biochem. Biophys.* **2014**, *557*, 47–54. [CrossRef] [PubMed]
6. Zhang, H.; Forman, H.J. 4-hydroxynonenal-mediated signaling and aging. *Free Radic. Biol. Med.* **2017**, *111*, 219–225. [CrossRef]
7. Morry, J.; Ngamcherdtrakul, W.; Yantasee, W. Oxidative stress in cancer and fibrosis: Opportunity for therapeutic intervention with antioxidant compounds, enzymes, and nanoparticles. *Redox Biol.* **2017**, *11*, 240–253. [CrossRef]
8. Bumbudsanpharoke, N.; Choi, J.; Park, I.; Ko, S. Facile biosynthesis and antioxidant property of nanogold-cellulose fiber composite. *J. Nanomater.* **2015**, *16*, 195. [CrossRef]
9. Du, L.; Suo, S.; Wang, G.; Jia, H.; Liu, K.J.; Zhao, B.; Liu, Y. Mechanism and cellular kinetic studies of the enhancement of antioxidant activity by using surface-functionalized gold nanoparticles. *Chem.-A Eur. J.* **2013**, *19*, 1281–1287. [CrossRef] [PubMed]
10. Nie, Z.; Liu, K.J.; Zhong, C.-J.; Wang, L.-F.; Yang, Y.; Tian, Q.; Liu, Y. Enhanced radical scavenging activity by antioxidant-functionalized gold nanoparticles: A novel inspiration for development of new artificial antioxidants. *Free Radic. Biol. Med.* **2007**, *43*, 1243–1254. [CrossRef]
11. Medhe, S.; Bansal, P.; Srivastava, M.M. Enhanced antioxidant activity of gold nanoparticle embedded 3,6-dihydroxyflavone: A combinational study. *Appl. Nanosci.* **2014**, *4*, 153–161. [CrossRef]
12. Vilas, V.; Philip, D.; Mathew, J. Essential oil mediated synthesis of silver nanocrystals for environmental, anti-microbial and antioxidant applications. *Mater. Sci. Eng. C* **2016**, *61*, 429–436. [CrossRef] [PubMed]
13. Popescu, R.C.; Andronescu, E.; Vasile, B.S. Recent advances in magnetite nanoparticle functionalization for nanomedicine. *Nanomaterials* **2019**, *9*, 1791. [CrossRef] [PubMed]
14. Alves, A.d.C.S.; Mainardes, R.M.; Khalil, N.M. Nanoencapsulation of gallic acid and evaluation of its cytotoxicity and antioxidant activity. *Mater. Sci. Eng. C* **2016**, *60*, 126–134. [CrossRef]
15. Salvador, M.; Gutiérrez, G.; Noriega, S.; Moyano, A.; Blanco-López, M.C.; Matos, M. Microemulsion synthesis of superparamagnetic nanoparticles for bioapplications. *Int. J. Mol. Sci.* **2021**, *22*, 427. [CrossRef]
16. Shah, S.T.; A Yehya, W.; Saad, O.; Simarani, K.; Chowdhury, Z.; A Alhadi, A.; Al-Ani, L.A. Surface functionalization of iron oxide nanoparticles with gallic acid as potential antioxidant and antimicrobial agents. *Nanomaterials* **2017**, *7*, 306. [CrossRef]
17. Shah, S.T.; Yehye, W.A.; Chowdhury, Z.Z.; Simarani, K. Magnetically directed antioxidant and antimicrobial agent: Synthesis and surface functionalization of magnetite with quercetin. *PeerJ* **2019**, *7*, e7651. [CrossRef]
18. Khan, S.; Shah, Z.H.; Riaz, S.; Ahmad, N.; Islam, S.; Raza, M.A.; Naseem, S. Antimicrobial activity of citric acid functionalized iron oxide nanoparticles -superparamagnetic effect. *Ceram. Int.* **2020**, *46*, 10942–10951. [CrossRef]
19. Ariffin, A.; Rahman, N.A.; Yehye, W.A.; Alhadi, A.A.; Kadir, F.A. Pass-assisted design, synthesis and antioxidant evaluation of new butylated hydroxytoluene derivatives. *Eur. J. Med. Chem.* **2014**, *87*, 564–577. [CrossRef]
20. Elmadfa, I.; Meyer, A.L. Body composition, changing physiological functions and nutrient requirements of the elderly. *Ann. Nutr. Metab.* **2008**, *52* (Suppl. S1), 2–5. [CrossRef]
21. Yehye, W.A.; Abdul Rahman, N.; Alhadi, A.A.; Khaledi, H.; Weng, N.S.; Ariffin, A. Butylated hydroxytoluene analogs: Synthesis and evaluation of their multipotent antioxidant activities. *Molecules* **2012**, *17*, 7645–7665. [CrossRef] [PubMed]

22. Daina, A.; Michielin, O.; Zoete, V. Swissadme: A free web tool to evaluate pharmacokinetics, drug-likeness and medicinal chemistry friendliness of small molecules. *Sci. Rep.* **2017**, *7*, 42717. [CrossRef]

23. Lagunin, A.; Stepanchikova, A.; Filimonov, D.; Poroikov, V. Pass: Prediction of activity spectra for biologically active substances. *Bioinformatics* **2000**, *16*, 747–748. [CrossRef] [PubMed]

24. Sotiriou, G.A.; Blattmann, C.O.; Deligiannakis, Y. Nanoantioxidant-driven plasmon enhanced proton-coupled electron transfer. *Nanoscale* **2016**, *8*, 796–803. [CrossRef] [PubMed]

25. Deligiannakis, Y.; Sotiriou, G.A.; Pratsinis, S.E. Antioxidant and antiradical sio2 nanoparticles covalently functionalized with gallic acid. *ACS Appl. Mater. Interfaces* **2012**, *4*, 6609–6617. [CrossRef]

26. Sahu, N.; Soni, D.; Chandrashekhar, B.; Sarangi, B.K.; Satpute, D.; Pandey, R.A. Synthesis and characterization of silver nanoparticles using cynodon dactylon leaves and assessment of their antibacterial activity. *Bioprocess Biosyst. Eng.* **2013**, *36*, 999–1004. [CrossRef]

27. Kumar, S.R.; Priyatharshni, S.; Babu, V.N.; Mangalaraj, D.; Viswanathan, C.; Kannan, S.; Ponpandian, N. Quercetin conjugated superparamagnetic magnetite nanoparticles for in-vitro analysis of breast cancer cell lines for chemotherapy applications. *J. Colloid Interface Sci.* **2014**, *436*, 234–242. [CrossRef]

28. De Faria, D.; Venâncio Silva, S.; De Oliveira, M. Raman microspectroscopy of some iron oxides and oxyhydroxides. *J. Raman Spectrosc.* **1997**, *28*, 873–878. [CrossRef]

29. Shebanova, O.N.; Lazor, P. Raman study of magnetite (Fe_3O_4): Laser-induced thermal effects and oxidation. *J. Raman Spectrosc.* **2003**, *34*, 845–852. [CrossRef]

30. Francisco, M.; Teresa, C.; María, C.; Ramón, P.; Rolando, R.; Pedro, F.; José María, S.; Eduardo, E.; Carmen, M. Synthesis and characterization of monodisperse magnetite hollow microspheres. *Soft Nanosci. Lett.* **2011**, *1*, 25–32.

31. Cornell, R.M.; Schwertmann, U. *The Iron Oxides: Structure, Properties, Reactions, Occurrences and Uses*; John Wiley & Sons: Hoboken, NJ, USA, 2006.

32. Dorniani, D.; Hussein, M.Z.B.; Kura, A.U.; Fakurazi, S.; Shaari, A.H.; Ahmad, Z. Preparation of fe3o4 magnetic nanoparticles coated with gallic acid for drug delivery. *Int. J. Nanomed.* **2012**, *7*, 5745–5756. [CrossRef] [PubMed]

33. Ma, H.-l.; Qi, X.-r.; Maitani, Y.; Nagai, T. Preparation and characterization of superparamagnetic iron oxide nanoparticles stabilized by alginate. *Int. J. Pharm.* **2007**, *333*, 177–186. [CrossRef] [PubMed]

34. Dorniani, D.; Bin, H.M.Z.; Kura, A.U.; Fakurazi, S.; Hussein-Al-Ali, S.H.; Shaari, A.H.; Ahmad, Z. In vitro sustained release study of gallic acid coated with magnetite-peg and magnetite-pva for drug delivery system. *Sci. World J.* **2014**, *2014*, 416354. [CrossRef] [PubMed]

35. Iyengar, S.J.; Joy, M.; Ghosh, C.K.; Dey, S.; Kotnala, R.K.; Ghosh, S. Magnetic, X-ray and mossbauer studies on magnetite/maghemite core-shell nanostructures fabricated through an aqueous route. *RSC Adv.* **2014**, *4*, 64919–64929. [CrossRef]

36. Zoete, V.; Daina, A.; Bovigny, C.; Michielin, O. Swisssimilarity: A web tool for low to ultra high throughput ligand-based virtual screening. *J. Chem. Inf. Modeling* **2016**, *56*, 1399–1404. [CrossRef]

37. Daina, A.; Zoete, V. A boiled-egg to predict gastrointestinal absorption and brain penetration of small molecules. *ChemMedChem* **2016**, *11*, 1117–1121. [CrossRef]

38. Tortosa, V.; Pietropaolo, V.; Brandi, V.; Macari, G.; Pasquadibisceglie, A.; Polticelli, F. Computational methods for the identification of molecular targets of toxic food additives. Butylated hydroxytoluene as a case study. *Molecules* **2020**, *25*, 2229. [CrossRef]